Effect of metal–support interaction on the selective hydrodeoxygenation of anisole to aromatics over Ni-based catalysts

Yongxing Yang [a], Cristina Ochoa-Hernández [a], Víctor A. de la Peña O'Shea [a], Patricia Pizarro [a,b], Juan M. Coronado [a,**], David P. Serrano [a,b,*]

[a] Thermochemical Processes Unit, IMDEA Energy Institute, Avenida Ramón de la Sagra, 3, Móstoles, 28935 Madrid, Spain
[b] Department of Chemical and Energy Technology, ESCET, Rey Juan Carlos University, c/Tulipán s/n, Móstoles, 28933 Madrid, Spain

ARTICLE INFO

ABSTRACT

Hydrodeoxygenation (HDO) of anisole has been often investigated in connection with biofuel production by bio-oil upgrading, because this molecule is representative of the methoxyphenyl components generated by flash pyrolysis of lignocellulose biomass. In the present work a series of Ni-containing (20 wt% loading) catalysts based on carriers as diverse as SBA-15, Al-SBA-15, γ-Al$_2$O$_3$, microporous carbon, TiO$_2$ and CeO$_2$ were selected in order to investigate the possible influence of metal–support interactions on the selectivity of anisole HDO toward aromatic products. Both, supports and catalysts were extensively characterized by N$_2$ adsorption–desorption isotherms, X-ray diffraction (XRD), transmission electron microscopy (TEM), H$_2$ temperature-programmed reduction (H$_2$-TPR) and ammonium programmed desorption (NH$_3$-TPD). Subsequently, the catalysts were tested for the hydrodeoxygenation of anisole in a continuous flow high pressure reactor. Under low hydrogen pressure (3 bars) and moderate temperature (290–310 °C) and space velocity (20.4 and 81.6 h^{-1}), these catalysts show a very high HDO activity that, for most of them approaches to 100%. Differences in product distribution among the catalysts are attributed not only to variations in the dispersion of the active phase, but also to the influence of the support properties in tuning its reactivity. In particular, acidity of the support is very relevant because strong acid sites may contribute the hydrogenolysis of anisole, while metallic sites will further hydrogenate intermediate compounds to yield cyclohexane. Therefore, the selective production of aromatics, from biomass derived feedstock in a biorefinery scheme can be promoted by an adequate selection of the catalysts characteristics. In this respect, a maximum yield of 64% of benzene was obtained in this study over Ni/C catalysts.

© 2013 Elsevier B.V. All rights reserved.

1. Introduction

Lignocellulose can be transformed by fast or flash pyrolysis, yielding up to 70% of a liquid fraction known as bio-oil, which can be used for biofuel production. However, the high oxygen content of this product leads to chemical instability, immiscibility with fossil fuels and corrosion, preventing the direct application of this liquid in the transportation sector [1]. Therefore, upgrading bio-oils to liquid hydrocarbons is an important milestone in the development of a feasible route for obtaining sustainable fuels from lignocellulose biomass [2]. Zeolite upgrading [3–7] and hydrotreating [8–11] are the two main approaches for bio-oil conversion, and accordingly these processes are being intensively studied. Though zeolites are effective in conversion of small oxygenates (such as aldehydes and ketones) through acid catalyzed reactions, their capability for deoxygenation of phenolic compounds derived from lignocellulose is limited due to extensive formation of coke [12]. Hydrodeoxygenation (HDO) at high pressure (30–50 bars) is an effective method to yield aliphatic hydrocarbons, but full hydrogenation of the aromatic ring of phenols and other aromatic chemicals over metal sites is inevitable under these conditions [8]. As a consequence the hydrogen consumption is high during these processes. Minimizing both carbon losses and also hydrogen demand (i.e. improving hydrogen efficiency) are important parameters for reducing the cost of biomass-derived liquids [13]. In this context, production of aromatic hydrocarbons such as toluene or benzene from the lignin fraction of biomass arises as an economically favorable process. Furthermore, arenes are important building blocks in petrochemical industry and replacing the feedstock from fossil to renewable resources in a biorefinery scheme is certainly advantageous.

* Corresponding author at: Thermochemical Processes Unit, IMDEA Energy Institute, Avenida Ramón de la Sagra, 3, Móstoles, 28935 Madrid, Spain.
** Corresponding author. Tel.: +34 917371120.
E-mail addresses: juanmanuel.coronado@imdea.org (J.M. Coronado), david.serrano@imdea.org (D.P. Serrano).

The aim of this work is to gain better understanding of the factors influencing the performance of the catalytic systems for the selective production of aromatic chemicals by bio-oil upgrading. In the present study anisole has been chosen as a molecule representative of those present in bio-oil obtained from feedstocks with high lignin content, because it contains a methoxy-phenyl moiety, which is characteristic of some of the main components of these liquids [14]. Furthermore, the relatively simple product distribution should facilitate the interpretation of the activity of the assayed catalysts. Previous studies on anisole hydrodeoxygenation were performed using catalysts based on Pt [15], Pt–Sn [16], metallic phosphides [17] or HZSM-5 and HY zeolites [18]. More recently, the use of non-sulfided Ni–Cu catalysts has been proposed as interesting alternative for hydrotreating bio-oils [19], while copper–chromite catalysts have been successfully applied to the HDO of a number of lignin model molecules [20]. In this line, the present work explores the capacity of the metal–support interaction to modulate the performance of Ni-based hydrotreating catalysts . With this aim, supports with properties as diverse as microporous carbon, γ-Al$_2$O$_3$, SBA-15, Al-SBA-15, TiO$_2$ and CeO$_2$ were selected for this study. These carrier materials are widely used to disperse active metals and they provide a variety of morphological and chemical characteristics, which can aid to determine the influence of textural properties, composition and acidity on modulating the characteristics of the Ni centers for the selective hydrodesoxygenation of anisole toward aromatics. In this respect, high surface carriers are expected to enhance metal dispersion at high loading, leading to an improved hydrogenation capacity. However, the metal distribution on the support will also depend on the specific surface interactions established during impregnation, such as those determined by the point of zero charge (PZC) of the solid. On the other hand, acid centers crucially determine catalytic behavior, and they have been reported to facilitate the hydrogenolysis of anisole and transmethylation reactions [18,20]. In addition, a moderate acidity of the support may promote the hydrogenation capacity of Ni [21]. Similarly, redox oxides such as TiO$_2$ may also contribute to promote HDO activity, as observed in bimetallic Ni–Cu catalysts [19].

2. Experimental

2.1. Catalysts preparation

For the synthesis of SBA-15, the structure-directing agent, Pluronic 123 (MW 5800, Aldrich), was dissolved in HCl solution at room temperature, and then heated to 40 °C before adding tetraethyl orthosilicate (TEOS; Aldrich), used as silica source. This mixture was stirred for 20 h at 40 °C, and aged at 100 °C for 24 h under autogeneous pressure. Thereafter, the solid product was recovered by filtration and dried overnight. The surfactant was removed by calcination at 550 °C for 5 h. Al-SBA-15 mesoporous material was synthesized according to the procedure described elsewhere [22], by adding to an aqueous solution of HCl at pH 1.5, TEOS and aluminum isopropoxide (Aldrich) in the proportion required to obtain a Si/Al ratio of 70. Subsequently, this solution was mixed with a second one containing Pluronic 123 solved in 150 ml of HCl at pH 1.5. The final mixture was stirred for 20 h at 40 °C and further treated under static conditions in an autoclave at 110 °C for 24 h. The solid product obtained was dried overnight and calcined in static air at 550 °C for 5 h with a rate of 1.8 °C/min. CeO$_2$ was prepared by direct calcination of Ce(NO$_3$)$_3$·6H$_2$O (Sigma–Aldrich) at 500 °C for 4 h. The rest of the supports were commercially available: microporous carbon (NORIT super 50), γ-Al$_2$O$_3$ (Alfa-Aesar), TiO$_2$ (Evonik-Degussa P25). In all cases the catalysts were prepared by wet impregnation of aqueous solutions of Ni(NO$_3$)$_2$·6H$_2$O

(Aldrich) in the amount required to get a final loading of 20 wt% Ni, followed by drying and calcination at 500 °C. For characterization purposes the calcined samples were reduced at 450 °C for 2 h in flowing H$_2$ (60 ml/min) and using a rate of 1 °C/min, then cooled down to room temperature under argon flow, and passivated by introducing progressively a stream of synthetic air at room temperature.

2.2. Catalysts characterization and testing

The nitrogen adsorption–desorption experiments were performed at 77 K on a Quadrasorb system. XRD patterns of the catalysts were recorded with a Philips PW 3040/00 X'Pert MPD/MRD diffractometer using Cu Kα radiation operated at 45 kV and 40 mA. TEM images of the catalysts were taken using a PHILIPS TECNAI 20T instrument, working at 200 kV and equipped with an EDX spectrometer for measuring X-ray energy dispersive spectra. The reducibility of the catalyst precursors was characterized by hydrogen temperature-programmed reduction (H$_2$-TPR), whereas acidity of the samples was determined by temperature programmed desorption of ammonium (NH$_3$-TPD). Both types of assays were performed in a Micromeritics AUTOCHEM 2910 equipment, loading 50-mg of sample in a quartz U-tube reactor. The TPR tests were conducted in a 10% H$_2$/Ar flow of 50 ml/min at a heating rate of 10 °C/min, and the hydrogen consumption was determined using a thermal conductivity detector (TCD). In the case of TPD experiments, the catalysts were first reduced in H$_2$ at 550 °C, and all the samples were outgassed in He at 350 °C, and finally saturated at 110 °C in a 15% NH$_3$/He stream (50 ml/min) for 45 min. After removing most weakly physisorbed NH$_3$ by flowing helium (50 ml/min) for 30 min, the chemisorbed ammonia was determined by using TCD by heating at 15 °C/min up to 550 °C under the same flow of helium.

The activity of the catalysts was studied in a fixed-bed tubular reactor (i.d. = 9 mm and l = 305 mm) with the catalyst bed placed upon a porous plate (Microactivity-Reference, PID Eng & Tech) operated at a pressure of 3 bars and a temperature ranging from 290 to 310 °C, with a feedstock containing anisole (Aldrich) in heptane (4 wt%). About 200 mg of catalyst pelletized, crushed and sieved with 40–60 mesh, and then mixed with silicon carbide were used in the assays. Before reaction, the catalysts were reduced in the reactor with a flow of pure hydrogen (60 ml/min) at 550 °C. During catalytic tests, the hydrogen flow rate was 30 ml/min and the organic phase was introduced at a rate of 6 ml/h or 24 ml/h, corresponding to a space velocity of 20.4 h^{-1} and 81.6 h^{-1}, respectively. Liquid samples collected at 1 h intervals were analyzed off-line by gas chromatograph (Agilent, 7890 A) equipped with a FID detector and HP-INNOWAX column for product analysis.

3. Results and discussion

3.1. Physicochemical characterization of the catalysts

In the present work a series of Ni-containing (20% loading) catalysts based on SBA-15, Al-SBA-15, γ-Al$_2$O$_3$, microporous carbon, TiO$_2$ and CeO$_2$ supports were prepared to determine the influence of metal–support interactions on the hydrotreating performance. In order to stabilize the activated form of the catalysts for characterization, they were previously reduced and passivated according to the procedure mentioned above. Textural properties of both the supports and the corresponding Ni-supported catalysts were obtained from the N$_2$ adsorption–desorption isotherms, which are displayed in Fig. 1, and the corresponding parameters are summarized in Table 1. Both, SBA-15 and Al-SBA-15 possess typical type IV sorption isotherms. However, while the hysteresis
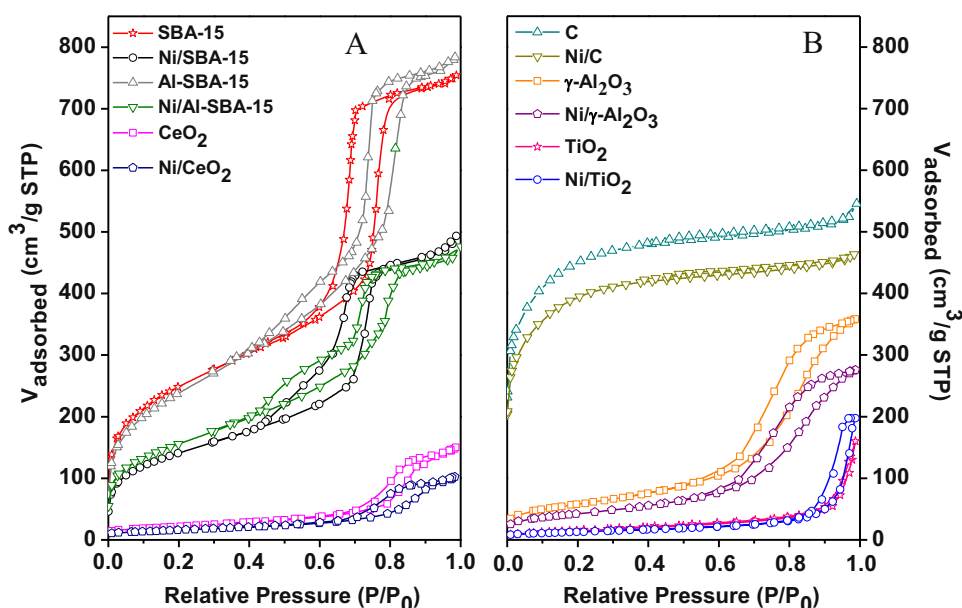
Fig. 1. N_2 adsorption–desorption isotherms of (A) SBA-15, Ni/SBA-15, Al-SBA-15, Ni/Al-SBA-15, CeO_2, Ni/CeO_2 and (B) C, Ni/C, γ-Al_2O_3, Ni/γ-Al_2O_3, TiO_2, Ni/TiO_2.

loop of the pure siliceous material is relative narrow, as expected for homogenous cylindrical pores, in the case of Al-SBA-15 the desorption branch (Fig. 1A) shows two steps, which indicates the presence of bottlenecks in the channels [23]. After the active metal was loaded in these two mesostructured supports, both the surface area and the pore volume were reduced in more than a 35%. This behavior is partly due to the fact that the relative high loading of the active component decreases the proportion of mesoporous SiO_2 in the catalysts, but it is also caused by the partial blockage of support pores due to the incorporation of nickel particles. In fact, this partial filling of the mesopores is reflected by a widening of the desorption branch, denoting certain narrowing of the channels. With regards to the pore size distribution (PSD) the value of Ni/SBA-15 obtained by BJH analysis shows a slight shift to lower diameter as compared with SBA-15, while the average diameter does not change appreciably for Ni/Al-SBA-15 catalyst. The isotherm of the Ni/γ-Al_2O_3 catalyst and that of the unmodified support also correspond to type IV isotherms, although the hysteresis loop is broader and shifted to higher pressures that in the mesostructured

supports (see Fig. 1A). This is due to a broader pore size distribution with slightly larger mean pore size. Incorporation of Ni on alumina slightly reduces both pore volume and surface area, in a proportion which matches the dilution effect due to the high metal loading. Samples based on carbon support display type I isotherms characteristic of microporous materials (see Fig. 1B), and, as in the other samples, the addition of Ni reduces moderately the pore volume and the specific surface area. Both Ni/TiO_2 catalysts and the corresponding support possess type II sorption isotherms with a small hysteresis loop at high relative pressures, characteristic of particulate materials. Finally, Ni/CeO_2 catalyst and the pure CeO_2 present isotherms which can be considered of type IV. The PSD results (not shown here) confirm that both CeO_2 and TiO_2 supports and the corresponding Ni catalysts are meso–macroporous materials, with a broad pore distribution due to interparticle voids. As in the previous cases, Ni impregnation lowers the pore volume and the specific surface area of Ni/CeO_2 with respect to the pure support. However, this effect is not observed in the case of Ni/TiO_2, which presents slightly larger pore size and volume than TiO_2.

Table 1
Physicochemical properties of supports and metal–supported catalysts.

Samples	S_{BET}[a] (m^2/g)	V_{total}[b] (cm^3/g)	Mesopore size[c] (nm)	Total acidity[d] (mequiv. NH_3/g)	Crystallite size[e] (nm)	
					Ni	MO_2
SBA-15	909	1.16	9.0	0.004	–	
Ni/SBA-15	513	0.76	8.1	0.099	20.3	
Al-SBA-15	870	1.21	8.0	0.021		
Ni/Al-SBA-15	563	0.73	8.0	0.212	20.0	
γ-Al_2O_3	209	0.55	9.3	0.107		
Ni/γ-Al_2O_3	153	0.43	9.3	0.213	7.6	
C	1608	0.84	–	0.043		
Ni/C	1410	0.72	–	0.099	8.8	
CeO_2	78	0.23	15.2	0.063		10.5
Ni/CeO_2	57	0.16	14.9	0.151	23.2	9.5
TiO_2	54	0.25	18.3	0.007	–	21.6[f]
Ni/TiO_2	46	0.31	26.8	0.064	16.7	22.0[f]

[a] BET surface area calculated from the adsorption branch of the N_2 isotherm.
[b] Total pore volumes calculated from the N_2 adsorption at relative pressure of 0.98.
[c] Mesopore diameter calculated from the adsorption branch using the BJH method.
[d] Total NH_3 desorption in the TPD.
[e] Crystallite size calculated from Scherrer's equation applied to the most intense diffraction peak.
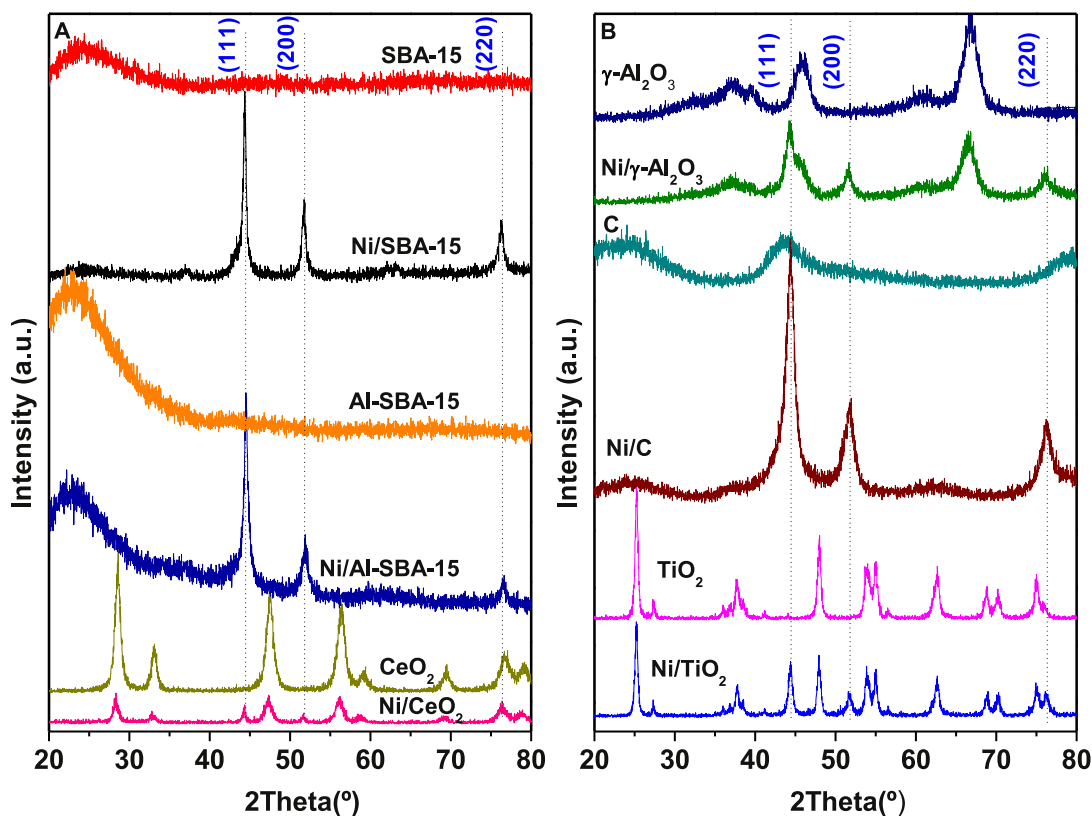[f] Corresponding to anatase phase.

Fig. 2. X-ray diffraction patterns of (A) SBA-15, Al-SBA-15, and CeO$_2$; (B) γ-Al$_2$O$_3$, carbon, and TiO$_2$ along with the corresponding Ni-loaded catalysts. Vertical dashed lines mark the main reflection of metallic nickel nanocrystals.

This behavior can be due to the significant contribution of the two types of particles, Ni and TiO$_2$, to the textural properties of Ni/TiO$_2$ catalyst.

The X-ray diffraction patterns of both supports and the corresponding Ni-supported catalysts are displayed in Fig. 2. γ-Al$_2$O$_3$ shows the characteristic broad peaks of this polymorph at 73.2°, 45.8° and 66.8° (JCPDS 010-0425). Microporous carbon is basically amorphous although it shows a very broad band at 43.7, which correspond to the (1 0 0) reflection of graphite (JCPDS 41-1487), and it indicates the existence of very small domains of this allotropic form of carbon. For both SBA-15 and Al-SBA-15 supports, the broad peak at around 22° is due to amorphous silica, as it is usually found for these mesostructured materials, which consist of an ordered array of channels in a non-crystalline matrix of SiO$_2$. This is confirmed by the low angle diffraction pattern of these materials (not shown). For TiO$_2$ support, diffraction peaks at 27° and 36° indicate the existence of the rutile crystallites (JCPDS 88-1175), while the diffraction peaks at 25°, 48°, 54°, 55°, 69° and 71° indicate the presence of anatase (JCPDS 84-1286), which is the majority phase in this support. Finally, the fluorite structure of CeO$_2$ can be identified by the peaks at 28.5, 33.0°, 47.5° and 56.3° (JCPDS 34-0394). In all cases, incorporation of Ni results in the appearance of new peaks at 44.4°, 51.7° and 76.3°, which correspond to crystallites of the face-centered cubic phase of this metal (JCPDS 04-0850). The diameters of Ni particles, as estimated by the Scherrer equation, are displayed in Table 1 for all the catalysts. These data reveal that, in the case of Ni/γ-Al$_2$O$_3$ and Ni/C catalyst the average size of the active phase is smaller than 9 nm, whereas for all the other catalysts are larger than 20 nm. In the case of Ni/SBA-15 and Ni/Al-SBA-15, the average diameter of the active phase (20.3 nm and 20.0 nm, respectively) is larger than the channel size (9 nm and 8 nm, respectively), suggesting than some particles are situated in the external surface, as confirmed by TEM. Finally, it is interesting to note that, while for

Ni/TiO$_2$ the size of both metallic and anatase particles is comparable, for Ni/CeO$_2$ the size of the metal particles is more than double than that of the support.

Fig. 3 displays some representative TEM images of the Ni/SBA-15, Ni/Al-SBA-15, Ni/TiO$_2$ and catalysts. In the former case (Fig. 3A), this TEM study reveals a significant heterogeneity in the size distribution of Ni particles, with large crystals (20–60 nm) outside the channels of the mesoporous silica and others significantly smaller and slightly elongated inside the pore structure. Similarly, in the case of Ni/Al-SBA-15, the TEM study (Fig. 3B) shows an uneven distribution of the metal particles sizes, with a significant contribution of relatively large particles (20–60 nm) on the external surface and a lower contribution of elongated particles in the channels. In general terms, the dispersion of the Ni in this sample is similar to the case of the Ni/SBA-15 catalysts, although the Ni particles in the external surface are slightly more uniform and the average diameter smaller than in the case of the pure siliceous support. In contrast, TEM images of the Ni/TiO$_2$ catalysts (Fig. 3C and D) show a more uniform size of the Ni particles, which are comparable in diameter (about 15–20 nm in the longer axis) to those of TiO$_2$. Both components, metallic and oxidic are in close contact and dark field images (not shown) confirm that the Ni particles are evenly distributed. A high resolution image of a Ni nanoparticle in contact with TiO$_2$ is displayed in Fig. 3D, presenting an irregular prismatic morphology with a longer axis of about 37 nm. A less clear distinction between components is observed in TEM images of the Ni/γ-Al$_2$O$_3$ catalysts (Fig. 3E and F), but some Ni particles of irregular, but mainly globular morphology, can be distinguished due to the darkest contrast. In general, small size metallic particles (<10 nm) in close contact with the support are observed for this sample. Fig. 4 shows the TEM images of the Ni/C, and Ni/CeO$_2$ catalysts. As it is evident from the micrographs of Fig. 4A and B, the metallic component is very homogeneously distributed on the carbon support. In this sample,
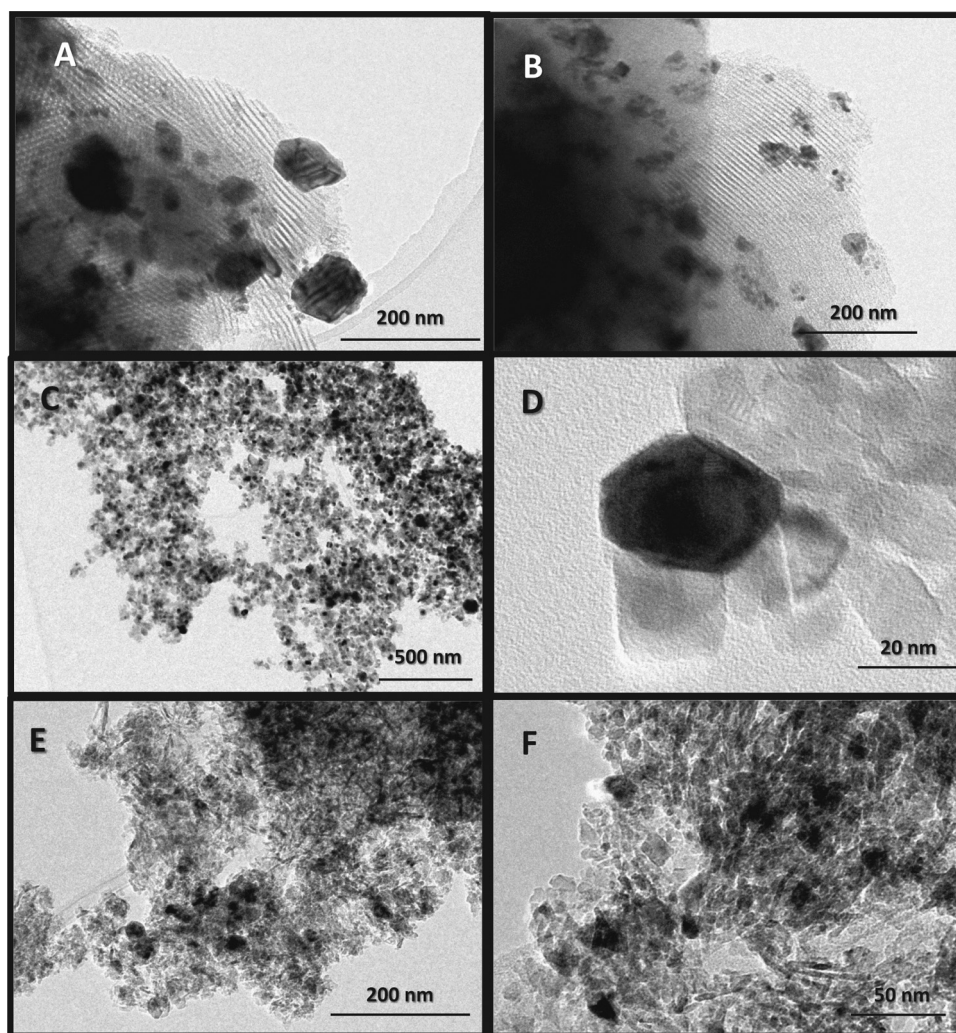
Fig. 3. TEM images of (A) Ni/SBA-15, (B) Ni/Al-SBA-15, (C) and (D) Ni/TiO$_2$, and (E) and (F) Ni/γ-Al$_2$O$_3$ catalysts.
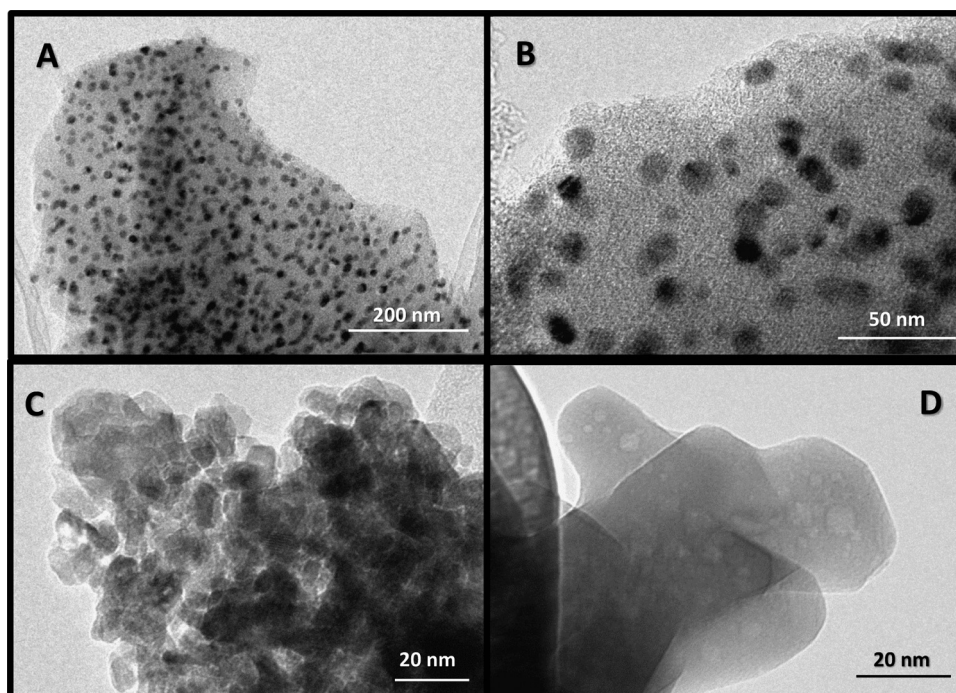

Fig. 4. TEM images of (A and B) Ni/C and (C and D) Ni/CeO$_2$, catalysts.
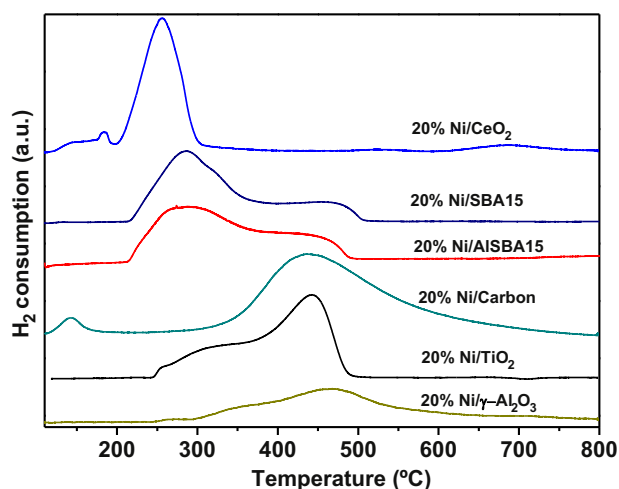
Fig. 5. TPR profiles of the precursors of Ni/CeO$_2$, Ni/SBA-15, Ni/Al-SBA-15, Ni/C, Ni/TiO$_2$ and Ni/γ-Al$_2$O$_3$ catalysts.

Ni particles present an almost spherical shape with a very narrow diameter distribution (12–18 nm). On the contrary, Ni/CeO$_2$ catalyst displays a more heterogeneous morphology at the nanoscale. As displayed in the image of Fig. 4C, this sample is constituted by an agglomeration of CeO$_2$ small nanoparticles (8–15 nm) with some large Ni particles unevenly distributed. The metallic particles of this catalyst, as identified by microanalysis, show an almost prismatic shape with dimensions in the 20–30 nm range (see Fig. 4D). Systematic XEDS microanalysis confirms the overall chemical composition of all the catalysts, although some heterogeneity in the distribution of the Ni is observed in most cases.

Fig. 5 compares the H$_2$-TPR profiles of the precursors of the catalysts used in this study. In the case of NiO/CeO$_2$ the main reduction feature is centered at 256 °C, which suggests a very weak interaction between the Ni and the CeO$_2$ because the reduction temperature obtained is the expected for the reduction of unsupported NiO [23]. For the NiO/SBA-15, the H$_2$ consumption peaks around 285 and 470 °C are attributed to the reduction of bulk NiO and nickel silicate, respectively, according to previous literature results [24]. Considering the relative intensity of these peaks, it seems that NiO particles with weak interaction with the support are majority. The reduction profile of NiO/Al-SBA-15 is very similar to the previous one, showing two main contributions at about 280 °C and 440 °C, which can be also related, respectively, to NiO particles with weak interactions with the support, and in closer contact with the siliceous matrix. The TPR results for these two mesostructured materials are consistent with the TEM study, which show for both Ni/Al-SBA-15 and Ni/SBA-15 catalysts the existence of metal particles in the external surface and, in lower proportion, smaller Ni particles inside the pores. On the other hand, in the case of precursor of the Ni/C catalysts a small peak at about 130 °C can be attributed to hydrogenation of carbon impurities, while the broad an intense feature at 440 °C can be related to the direct reduction of the nitrate precursor to Ni^0 because, in contrast with the other cases, this material was not calcined after impregnation. For NiO/TiO$_2$, the broad reduction peak at around 300 °C, arising from the reduction of bulk NiO particles is similar to that observed for other catalysts. However the main reduction peak centered at 440 °C is ascribed to the formation of Ni^0 species in close contact with the TiO$_2$ support [25]. In the case of NiO/γ-Al$_2$O$_3$ a broad peak with a maximum at 446 °C and a shoulder at 361 °C can be observed. This profile indicates the existence of a majority of strongly interacting nickel species, which gives rise to the high temperature feature. However, the relative low intensity of the TPR curve suggests that hardly reducible

species such as NiAl$_2$O$_4$ are also present in this sample [26]. In summary, the TPR results indicate that, except Ni/CeO$_2$, Ni/SBA-15 and Ni/Al-SBA-15 catalysts, all the studied samples present significant metal–support interactions.

These results reveal that, in general terms, dispersion of Ni is higher in large surface area supports such as carbon or alumina, than on oxides of relatively low specific surface such as CeO$_2$ and TiO$_2$. Nevertheless, other surface and morphological features also influence the final size of the metal; thus, catalysts with specific metal–support interaction such as Ni/C give rise to a very homogenous distribution of metallic nanoparticles. In this respect, it is worth noting that previous studies have revealed that Ni adsorption is favored by the acidity of the carbon support [27]. In other cases, such as the catalyst based on SBA-15, the relatively weak metal–support interaction and the influence of the mesostructure create in an almost bimodal distribution of Ni, with large globular particles outside the pores and elongated one inside channels. However, in contrast with previous reports [28], the metal distribution is similar for Ni/SBA-15 and Ni/Al-SBA-15 catalysts, despite the expected differences in acidity. This behavior is very likely related to the high Ni-loading of these catalysts, which exceed by large the number of acid sites created by the Al-incorporation.

The acidity of both catalysts and supports was determined by thermo-programmed desorption of ammonia (NH$_3$-TPD). The desorption profiles for all the Ni-supported catalysts are displayed in Fig. 6, while the total amount of NH$_3$ adsorbed for catalysts and supports are summarized in Table 1. These results reveal that both Ni/SBA-15 and Ni/TiO$_2$ present a moderate amount of weak acid sites, as evidenced by the small desorption peaks centered at around 260 °C and 270 °C, respectively. Considering that, neither SBA-15 nor TiO$_2$ show this desorption feature, the presence of these weak acid sites must be related to centers created by the incorporation of the metal. In this respect, it has been previously reported that Ni incorporation results in the formation of additional acid sites [29], which accordingly with the relatively large amount of metal is very significant in these catalysts (see Table 1). Furthermore, intense TPD peaks at about 280 °C have observed in other catalytic systems containing high loading of Ni [30]. Modification of the SBA-15 with Al yields to a significant increment of the acidity of both the support and the corresponding catalysts. In this way Ni/Al-SBA-15 presents a peak at 270 °C, which is appreciably larger than the equivalent one for Ni/SBA-15. Similarly, Ni/γ-Al$_2$O$_3$ presents a prominent peak at about 278 °C, associated with weak acidic sites and a broader, less intense feature at 458 °C, which can be attributed to stronger acid sites. On the other hand, the pure CeO$_2$ show only a
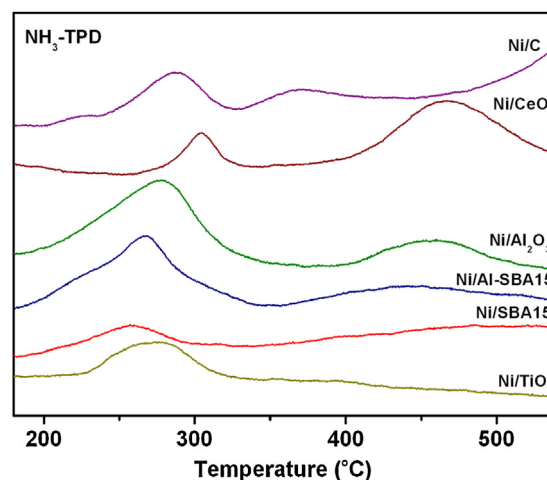

Fig. 6. NH$_3$-TPR profiles of the of Ni/C, Ni/CeO$_2$, Ni/γ-Al$_2$O$_3$, Ni/Al-SBA-15, Ni/SBA-15, and Ni/TiO$_2$ catalysts.

weak NH$_3$ desorption feature at about 440 °C (not shown). This feature is most likely related with the presence of surface impurities, because it has been reported that this oxide presents strong basic sites [31]. In contrast Ni/CeO$_2$ sample shows two well-defined peaks, one smaller at 304 °C and other broader at 476 °C. As in other cases, the low temperature feature can be associated to weak acidic sites formed by Ni incorporation, while the high temperature desorption should correspond to stronger centers, possibly related to the formation of acidic sites in the interface between the two components. Finally, Ni/C catalyst shows two main desorption peaks at 295 °C and 360 °C, while the TPD of the pure support present only a broad peak centered at about 420 °C. These features can be tentatively assigned to weak and medium strength acid sites formed on Ni particles and the Ni/C carbon interface, respectively. In summary, from the NH$_3$-TPD it can be concluded that that acidity of these catalysts is greatly influenced by Ni incorporation,

which generates mainly weakly acidic sites although in the case of Ni/CeO$_2$, Ni/γ-Al$_2$O$_3$ and Ni/C, some stronger sites are also present.

3.2. Catalytic activity

The main products of anisole hydrodeoxygenation are cyclohexane, benzene and n-hexane, although some oxygenated compounds such as methylcyclohexane, cyclohexanone, cyclohexanol or phenol are also found. Fig. 7 displays the evolution with the time on stream of the anisole conversion and the selectivity for the catalysts assayed at 290 °C and 3 bars of pressure. Under these conditions, full conversion is obtained only for Ni/SBA-15, Ni–Al-SBA-15 and Ni/γ-Al$_2$O$_3$, while for Ni/C it reaches 98%. In contrast, anisole conversion over Ni/CeO$_2$ is lower than 90% and it reaches only 47% for Ni/TiO$_2$. However, it can be observed that conversion is very stable in the time interval of these catalytic tests,
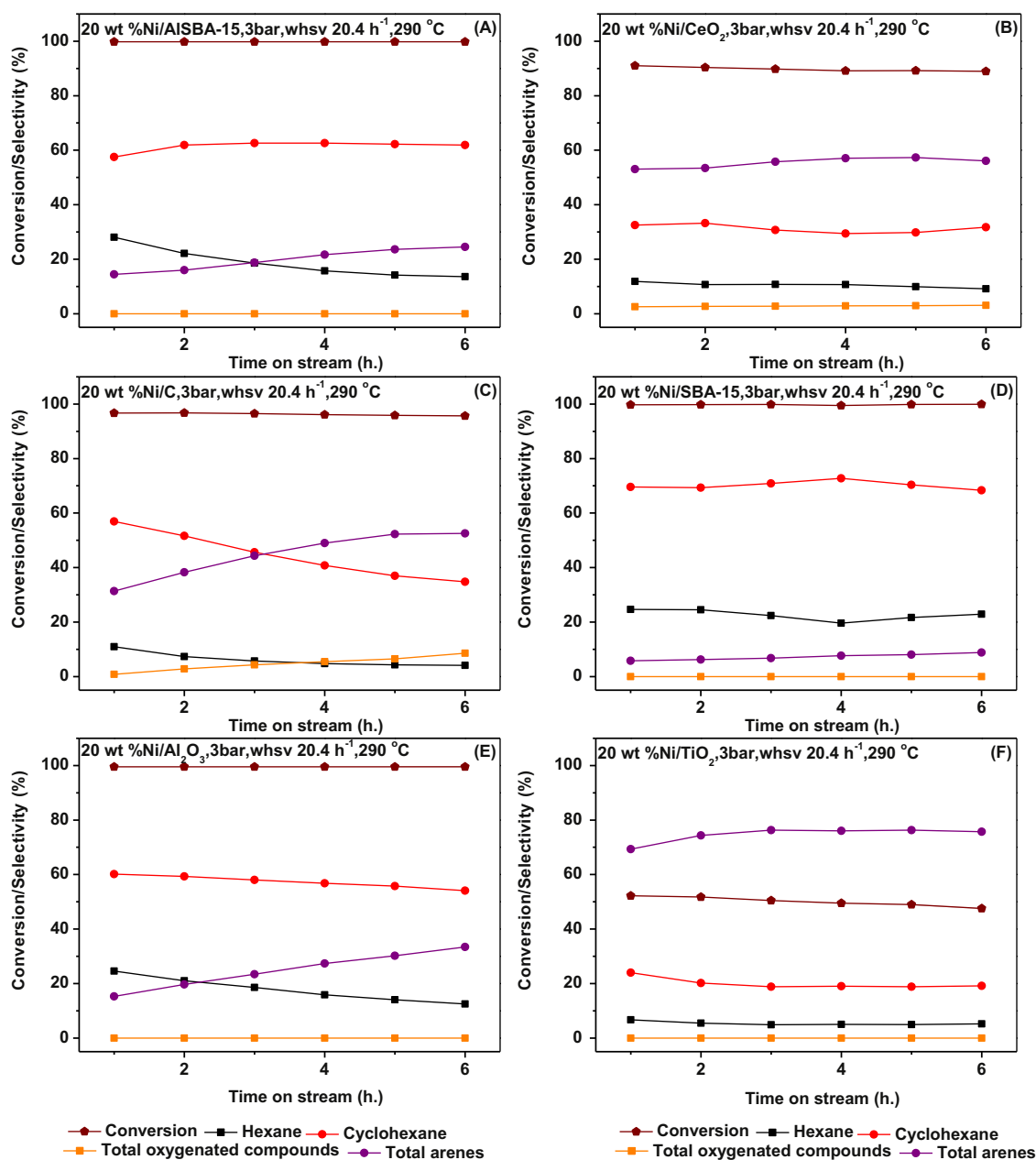

Fig. 7. Evolution with the time on stream of the anisole conversion and the selectivity to cyclohexane, n-hexane, aromatic and oxygenated compounds for the (A) Ni/Al-SBA-15, (B) Ni/CeO$_2$, (C) Ni/C, (D) Ni/SBA-15, (E) Ni/γ-Al$_2$O$_3$ and (F) Ni/TiO$_2$ catalysts used in this study. Reaction conditions: 3 bars, 290 °C, WHSV: 20.4 h^{-1}, H$_2$/feedstock ratio: 300 Nm^3/m^3.

although Ni/TiO$_2$ catalyst shows a slight decline in the activity with time on stream. Under these conditions, Ni/CeO$_2$ and especially Ni/C catalysts produce minor amount of oxygenated compounds (<10%), mainly methoxycyclohexane and cyclohexanone. However, the hydrodeoxygenation (HDO) efficiency approaches 100% for the other catalysts. With regard to the hydrocarbon distribution, selectivity to cyclohexane reaches almost 70% in the case of the Ni/SBA-15 and it is close to 62% in the case of Ni/Al-SBA-15. For these two catalysts the production of n-hexane is also significant, especially for Ni/SBA-15, which presents a selective toward this linear alkane of about 22%. Cyclohexane and n-hexane are also the main products of HDO over Ni/γ-Al$_2$O$_3$. In contrast, the other catalysts, such as Ni/CeO$_2$, generate mainly benzene, and for Ni/TiO$_2$ the selectivity toward aromatics is about 75% under these conditions. In addition, Ni/C, Ni/Al-SBA-15 and Ni/γ-Al$_2$O$_3$ show a progressive increment of the selectivity toward benzene at the expenses of cyclohexane production. This fact suggests that moderate loss of hydrogenation capacity, most likely due to carbon deposition on Ni sites, can have a positive effect for aromatic production. Although direct comparisons with previous works are complex due to the diversity of reaction conditions employed, it seems that Ni-based catalysts present efficiencies for HDO comparable to that reported in the literature, but the selectivity to benzene is significantly enhanced for the catalysts investigated in this study [15–18,32]. In this respect, the catalysts based on reducible oxides such as Ni/TiO$_2$ and Ni/CeO$_2$, as well as Ni/C show a remarkable selectivity toward aromatics.

Fig. 8 shows the yield toward the products of anisole hydrotreating over the different catalysts after 6 h on stream at two different temperatures and space velocities. The product distribution for all these tests is summarized in the Table 2. At 20.4 h^{-1} of space velocity the increment of the reaction temperature from 290 to 310 °C (see Fig. 8A and B) leads to a remarkable change in the product distribution, which is particularly dramatic over Ni/Al-SBA-15, Ni/SBA-15, and Ni/γ-Al$_2$O$_3$ catalysts. Thus, whereas at lower temperature the main product of the anisole hydrotreating is cyclohexane, at higher temperature these samples produce significantly more n-hexane and benzene. For the other catalysts the variation in the products yield show a similar trend, with a significant increase of the selectivity toward n-hexane at expenses of cyclohexane when increasing the operation temperature. In addition, the general increment of arene yield at 310 °C achieves a maximum value of about 65% over Ni/C. On the other hand, the increment of the space velocity reduces, as expected, the overall yields because the anisole conversion decreases (see Fig. 8B–D). Furthermore, this parameter has a stronger effect on cyclohexane production, which is greatly reduced at 81.6 h^{-1}. Thus, for example, cyclohexane yield at 290 °C over Ni/SBA-15 drops to one sixth by increasing the space velocity from 20.4 to 81.6 h^{-1}. In parallel, the yield of benzene shows a four-fold increment over this catalyst. In contrast a significant decline of aromatic production is observed for Ni/TiO$_2$ and, in a lower extent, for Ni/C and Ni/CeO$_2$. Toluene is also produced in small proportion over Ni/γ-Al$_2$O$_3$ at the larger space velocity. Finally, it is worth, mentioned that increasing the space velocity results in a slight increment of the yield to oxygenated molecules such as methoxycyclohexane over Ni/SBA-15, Ni/C and Ni/CeO$_2$ catalysts. Accordingly, the HDO yield of these catalysts is appreciably lower under these conditions. On the other hand, rising the temperature up to 310 °C enhances the yield to aromatic products over all the catalysts with respect to the results obtained at 290 °C
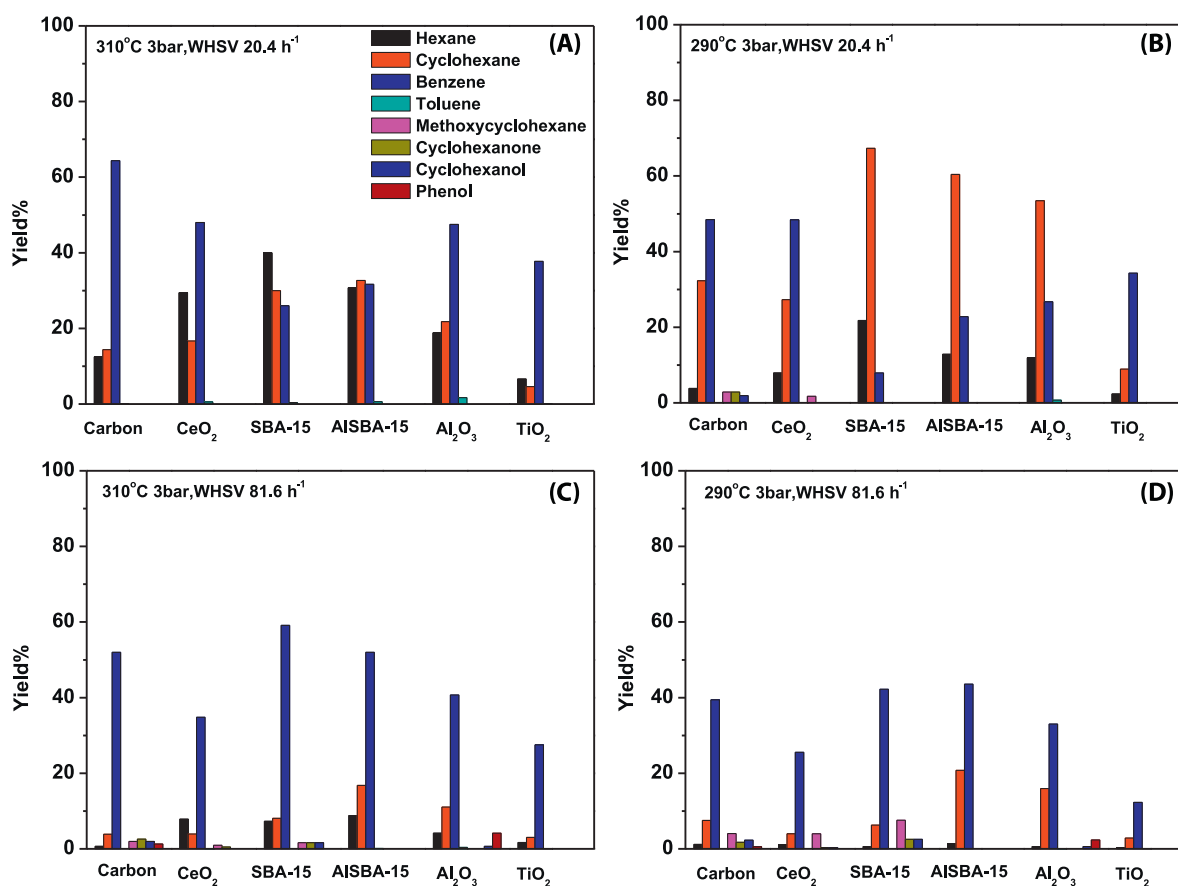

Fig. 8. Yield to the different products of anisole HDO over the studied catalyst at 3 bar of pressure at (A and C) 290 °C; or (B and D) 310 °C, at WHSV (A and B) 20.4 h^{-1} or (C and D) 81.6 h^{-1}.
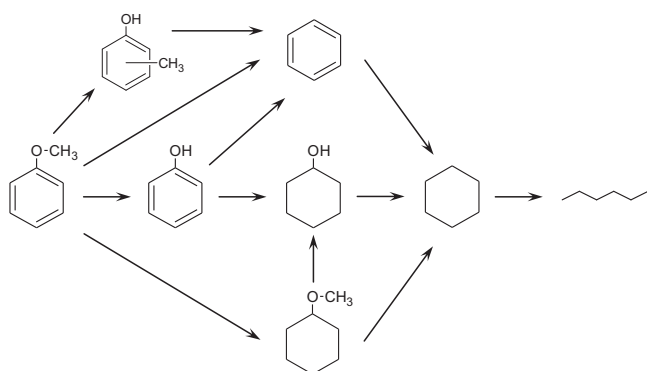
Table 2
Products distribution of the anisole hydrotreating after 6 h on stream over different catalysts and operating conditions.

Conditions	Catalysts	$X_{anisole}$	S_{hexane}	$S_{cyclo-hexane}$	$S_{benzene}$	$S_{toluene}$	$S_{methoxy-cyclohexane}$	$S_{cyclo-hexanone}$	$S_{cyclo-hexanol}$	S_{phenol}	HDO%
310 °C, 3 bar, WHSV 20.4 h⁻¹	Ni/C	96	13	15	67	1	0	0	0	0	100
	Ni/CeO₂	98	30	17	49	2	0	0	0	0	100
	Ni/SBA-15	100	40	30	26	1	0	0	0	0	100
	Ni/Al-SBA-15	99	31	33	32	2	0	0	0	0	100
	Ni/Al₂O₃	99	19	22	48	9	0	0	0	0	100
	Ni/TiO₂	51	13	9	74	2	0	0	0	0	100
290 °C, 3 bar, WHSV 20.4 h⁻¹	Ni/C	95	4	34	51	0	3	3	2	0	92
	Ni/CeO₂	88	9	31	55	0	2	0	0	0	100
	Ni/SBA-15	99	22	68	8	0	0	0	0	0	100
	Ni/Al-SBA-15	99	13	61	23	0	0	0	0	0	100
	Ni/Al₂O₃	99	12	54	27	6	0	0	0	0	100
	Ni/TiO₂	47	5	19	73	1	0	0	0	0	100
310 °C, 3 bar, WHSV 81.6 h⁻¹	Ni/C	65	1	6	80	0	3	4	3	2	87
	Ni/CeO₂	49	16	8	71	1	2	1	0	0	96
	Ni/SBA-15	81	9	10	73	0	2	2	2	0	92
	Ni/Al-SBA-15	80	11	21	65	1	0	0	0	0	99
	Ni/Al₂O₃	69	6	16	59	9	0	0	1	6	92
	Ni/TiO₂	34	5	9	81	1	0	0	0	0	99
290 °C, 3 bar, WHSV 81.6 h⁻¹	Ni/C	58	2	13	68	0	7	3	4	1	84
	Ni/CeO₂	36	3	11	71	0	11	1	1	0	86
	Ni/SBA-15	63	1	10	67	0	12	4	4	0	79
	Ni/Al-SBA-15	67	2	31	65	0	0	0	0	0	99
	Ni/Al₂O₃	59	1	27	56	8	0	0	1	4	94
	Ni/TiO₂	16	2	18	77	1	0	0	0	0	99

when operating at 81.6 h⁻¹ of space velocity (see Fig. 8C and D). In this respect, the highest aromatic yield is obtained under these conditions for all the catalysts, except for Ni/CeO₂ and Ni/C.

In accordance with previous works [17,20], these results suggest that anisole transformation under hydrotreating conditions occurs by a complex network of reactions. Formation of cyclohexane at low temperature and reduced space velocity indicates that anisole deoxygenation takes place via demethylation and subsequent hydrogenation (see scheme of Fig. 9) [16]. The existence of this chain of transformations is further supported by the detection of phenol intermediates [18]. This oxygenated compound is mainly found in small concentration over Ni/γ-Al₂O₃. On the other hand, direct hydrogenation of anisole without demethylation can be inferred by the presence of methoxycyclohexane, which has been previously detected when using copper chromite as catalysts [20]. In the present work, methoxycyclohexane is mainly detected as minor product on Ni/C, Ni/CeO₂ and Ni/SBA-15 at low temperature and high space velocity. On the other hand, the significant production of benzene points out to the contribution of a different demethylation pathway, which is activated at higher temperature, as previously reported [20]. Similarly, formation of minor amounts of toluene may occur throughout transmethylation

and hydrogenation, while cresol will be generated by successive transmethylation and hydrogenolysis [19]. Obviously, further hydrogenation of the aromatic ring is also possible and it will lead to cyclohexane production. Subsequently, cyclohexane can undergo hydrogenolysis to yield n-hexane, as it has been reported over Rh and Ir catalysts [33]. It has been previously suggested that these two main routes of anisole transformation can be driven by differences in the adsorption configuration of substrate molecule [20]. Thus, adsorption through the oxygen bond may favor demethylation, whereas π-bond adsorption leads to the hydrogenation of the aromatic ring. Therefore, differences in the surfaces properties of the catalysts should explain the variations in selectivity.

According to the activity results, in general, the support seems to have significant influence in modulating the selectivity of the HDO of anisole. However, the catalytic behavior of both Ni/SBA-15 and Ni/Al-SBA-15 catalysts is relatively similar, suggesting that it mainly determined by metallic sites. In fact, as mentioned in section 3.1, incorporation of Al has relatively small effect on the acidity most likely due to high metal loading. These two catalysts present an elevated hydrogenation capacity, and at high temperature promote the cycle opening to yield n-hexane, particularly Ni/SBA-15. In the case of Ni/TiO₂, despite the similar size of the particles of the metal and the oxide there is a significant interaction between both components, as revealed by TPR results. According with previous reports, this strong metal–support interaction reduces the hydrogenation capacity [34], and this can justify the reduced yield to saturated hydrocarbon obtained with this catalyst. In fact, this catalyst shows the highest selectivity toward aromatic, although the overall yield is lower than for other catalysts. Despite the fact that CeO₂ is also a reducible oxide, metal support interactions are not very significant in this catalyst, judging by the TPR results. In fact, this catalyst shows both hydrogenation capacity of the aromatic ring, which can be favored by the relatively large Ni particles of this material, and a significant yield to benzene. In this respect, formation of aromatics can be promoted by the hydrogenolysis of anisole on relatively strong acid sites. This route seems to be also relevant for Ni/γ-Al₂O₃, as suggested by the detection of phenol, but the hydrogenation capacity of this catalyst is larger than that of

Fig. 9. Scheme of the possible routes for anisole hydrodeoxygenation.

Ni/CeO$_2$. Thus, strong acid sites may contribute the hydrogenolysis, while metallic sites will further hydrogenate intermediate compounds to yield cyclohexane. On the other hand, the acidity of the Ni/γ-Al$_2$O$_3$ catalyst may also explain the formation of toluene by transmethylation [17]. Combination of strong acidic sites and good dispersion of the metal leads to a very good aromatic yield over the Ni/C catalyst, especially at high temperature. Al low temperature, Ni/C presents a relatively low HDO yield, due to the moderate capacity for the hydrogenation of the C—O bonds. In summary, the balance of metallic sites, acidic centers, as well as the redox characteristic of the supports can contribute to modulate the selectivity of these HDO catalysts.

4. Conclusions

In this work, a series of different Ni-based catalysts with a broad range of physicochemical properties were prepared and tested for the hydrodeoxygenation of anisole. All these catalysts show high activity and excellent selectivity toward benzene production under relatively low hydrogen pressure (3 bars) and moderate temperatures (290–310 °C). Regarding aromatic production, better results are obtained at higher temperature and lower space velocity. Significant differences of the product distribution are observed among the used catalysts, which can be attributed to differences in the active phase distribution, but also to the contribution of the effect support. In particular, acidity of the support is very relevant because strong acid sites may contribute the hydrogenolysis of anisole, while metallic sites will further hydrogenated intermediate compounds to yield cyclohexane. Thus, combination of strong acidic sites and good dispersion of the metal leads to a very good aromatic yield over the Ni/C catalyst, in lower extent over Ni/γ-Al$_2$O$_3$, especially at high temperature. On the other hand, Ni/SBA-15 and Ni/Al-SBA-15 catalysts, which present weak acidity and large Ni particles, show an elevated hydrogenation capacity and, at high temperature, promote the cycle opening to yield n-hexane. Ni/CeO$_2$ catalysts present an intermediate situation with high selectivity to aromatics and n-hexane. Finally, the strong metal–support interactions on Ni/TiO$_2$ lead to a limited anisole conversion, but with a high selectivity toward benzene. Therefore, it can be concluded that the selective production of aromatics from biomass derived feedstock in biorefinery scheme can be promoted by an adequate selection of the catalysts characteristics.

Acknowledgements

References

[1] G.W. Huber, S. Iborra, A. Corma, Chemical Reviews 106 (2006) 4066.
[2] S. Stocker, Angewandte Chemie. International Edition in English 47 (2008) 9200.
[3] A.G. Gayubo, A.T. Aguayo, A. Atutxa, R. Aguado, J. Bilbao, Industrial and Engineering Chemistry Research (2004) 2610.
[4] P.D. Chantal, S. Kaliaguine, J.L. Grandmaison, Applied Catalysis 18 (1985) 133.
[5] P.A. Horne, P.T. Williams, Renewable Energy 7 (1996) 131.
[6] J.D. Adjaye, N.N. Bakhshi, Biomass and Bioenergy 8 (1995) 131.
[7] X.L. Zhu, R.G. Mallinson, D.E. Resasco, Applied Catalysis A 279 (2010) 181.
[8] C. Zhao, Y. Kou, A.A. Lemonidou, X.B. Li, J.A. Lercher, Angewandte Chemie International Edition 48 (2009) 3987.
[9] C.A. Fisk, T. Morgan, Y.Y. Ji, M. Crocker, C. Crofcheck, S.A. Lewis, Applied Catalysis A 358 (2009).
[10] A. Gutierrez, R.K. Kaila, M.L. Honkela, R. Slioor, A.O.I. Krause, Catalysis Today 147 (2009) 239.
[11] D.Y. Hong, S.J. Miller, P.K. Agrawal, C.W. Jones, Chemical Communications 46 (2010) 1038.
[12] T.P. Vispute, H. Zhang, A. Sanna, R. Xiao, G.W. Huber, Science 330 (2010) 1222.
[13] J.Q. Bond, D.M. Alonso, D. Wang, R.M. West, J.A. Dumesic, Science 327 (2010) 1110.
[14] M. Garcia-Perez, A. Chaala, H. Pakdel, D. Kretschmer, C. Roy, Biomass and Bioenergy 31 (2007) 222–242.
[15] R.C. Runnebaum, T. Nimmanwudipong, D.E. Block, B.C. Gates, Catalysis Letters 141 (2011) 817–820.
[16] M.A. Gonzalez-Borja, D.E. Resasco, Energy and Fuels 25 (2011) 4155–4162.
[17] K. Li, R. Wang, J. Chen, Energy and Fuels 25 (2011) 854–863.
[18] T. Prasomsri, A.T. Toa, S. Crossley, W.E. Alvarez, D.E. Resasco, Applied Catalysis B 106 (2011) 204–211.
[19] A.R. Ardiyanti, S.A. Khromova, R.H. Venderbosch, V.A. Yakovlev, H.J. Heeres, Applied Catalysis B 117–118 (2012) 105–117.
[20] K.L. Deutsch, B.H. Shanks, Applied Catalysis A 447 (2012) 144–150.
[21] S. Hu, M. Xue, H. Chen, J. Shen, Chemical Engineering Journal 162 (2010) 371–379.
[22] Y. Yue, A. Gédéon, J. Bonardet, N. Melosh, J. D'Espinose, J. Fraissard, Chemical Communications (1999) 1967–1968.
[23] N. Lin, J.Y. Yang, Z.Y. Wu, H.J. Wang, J.H. Zhu, Microporous and Mesoporous Materials 139 (2011) 130–137.
[24] Y. Wang, A. Zhu, Y. Zhang, C.T. Au, X. Yang, C. Shi, Applied Catalysis B 81 (1–2) (2008) 141–149.
[25] J. Loosdrecht, M. van der Kraan, A.J. van Dillen, J.W. Geus, Journal of Catalysis 170 (1997) 217.
[26] B. Roy, K. Loganathan, H.N. Pham, A.K. Datye, C.A. Leclerc, International Journal of Hydrogen Energy 35 (21) (2010) 11700–11708.
[27] S. Wang, G.Q. Lu, Carbon 36 (1998) 283–292.
[28] C. Ochoa-Hernández, Y. Yang, P. Pizarro, V.A. de la Peña O'Shea, J.M. Coronado, D.P. Serrano, Catalysis Today, in press
[29] K. Fang, J. Ren, Y. Sun, Journal of Molecular Catalysis A: Chemical 229 (2005) 51–58.
[30] P. Castaño, B. Pawelec, J.L.G. Fierro, J.M. Arandes, J. Bilbao, Fuel 86 (2007) 2262–2274.
[31] E.I. Gürbüz, E.L. Kunkes, J.A. Dumesic, Applied Catalysis B 94 (2010) 134–141.
[32] C.V. Loricera, B. Pawelec, A. Infantes-Molina, M.C. Álvarez-Galván, R. Huirache-Acuña, R. Nava, J.L.G. Fierro, Catalysis Today 172 (2011) 103–110.
[33] G. Rodríguez-Gattorno, L.O. Alemán-Vázquez, X. Angeles-Franco, J.L. Cano-Dominguez, R. Villagómez-Ibarra, Energy and Fuels 21 (2007) 1122–1126.
[34] J. van de Loosdrecht, A.M. van der Kraan, A.J. van Dillen, J.W. Geus, Journal of Catalysis 170 (1997) 217–226.